Adhesion force in fluids: Effects of fingering, wetting, and viscous normal stresses

Pedro H. A. Anjos, Eduardo O. Dias, Laércio Dias, and José A. Miranda*
Departamento de Física, Universidade Federal de Pernambuco, Recife, Pernambuco 50670-901, Brazil
(Received 30 October 2014; published 7 January 2015)

Probe-tack measurements evaluate the adhesion strength of viscous fluids confined between parallel plates. This is done by recording the adhesion force that is required to lift the upper plate, while the lower plate is kept at rest. During the lifting process, it is known that the interface separating the confined fluids is deformed, causing the emergence of intricate interfacial fingering structures. Existing meticulous experiments and intensive numerical simulations indicate that fingering formation affects the lifting force, causing a decrease in intensity. In this work, we propose an analytical model that computes the lifting adhesion force by taking into account not only the effect of interfacial fingering, but also the action of wetting and viscous normal stresses. The role played by the system's spatial confinement is also considered. We show that the incorporation of all these physical ingredients is necessary to provide a better agreement between theoretical predictions and experiments.

DOI: 10.1103/PhysRevE.91.013003 PACS number(s): 47.20.Ma, 47.15.gp, 68.35.Np, 68.15.+e

I. INTRODUCTION

The study of the adhesion properties of viscous fluids has been the object of a lot of research in recent years [1–16]. In all these investigations a key factor is the precise evaluation and characterization of the bond strength of spatially confined, liquid thin films. This can be achieved through the employment of an adhesion test, commonly known as the probe-tack test [17,18]. In this test, a fluid sample is placed between two closely spaced parallel flat plates, and then the upper plate is lifted vertically at a prescribed rate. This happens while the lower plate is held fixed. During this fluid-stretching process the applied lifting force is recorded. The result of such measurement is an adhesion force curve that quantifies the adhesive response of the liquid sample as a function of the upper plate displacement, or lifting time.

In addition to the assessment of the lifting adhesion force, another aspect of the problem has also been intensively investigated, both experimentally and theoretically [19–32]. It refers to the study of the appealing pattern formation phenomenon that takes place at the interface separating the lifted, more viscous fluid (e.g., oil), and the surrounding fluid (for instance, air) during the lifting procedure. As the plates separate, the outer less-viscous fluid enters the system, and the more-viscous inner fluid moves inward. As a result, the fluid-fluid interface deforms, assuming complex, visually striking interfacial morphologies. The development of such interfacial instabilities is reminiscent of the classic viscous fingering instability [33], associated with the celebrated Saffman-Taylor problem [34]. The lifting setup examined in Refs. [19–32] is also known as the lifting Hele-Shaw cell problem.

One interesting aspect that connects the research performed in Refs [1–18] (evaluation of the adhesion force) and that of Refs. [19–32] (study of the emerging pattern-forming structures) is the influence of fingering formation on the determination of the adhesion force itself. This important issue has been addressed via experiments and numerical simulations in Refs. [2,3,9,14]. Initially, Derks *et al.* [2] have found a good agreement between their theoretical expression for the lifting force (that considered the interface as a stable retracting circle) and their experimental results. At that time, these authors argued that the detailed shape of the interface should have a very modest, or even no influence at all on the adhesive force. However, by dealing with highly viscous oils and larger lifting-plate velocities, the experiments performed by Poivet *et al.* [3] have found that the fingering mechanism has indeed an influence on the lifting force. Afterwards, the influence of interfacial fingering on the adhesion force has been supported by the intensive numerical simulations carried out in Ref. [9] by Lindner and coworkers, and then confirmed by the meticulous experimental investigation recently conducted in Ref. [14] by Nase and collaborators. The main conclusion of these analyses was that the fingering formation process is in fact responsible for a decrease in the adhesion force.

Despite all the useful information and valuable advances obtained from the experimental and numerical studies performed in Refs. [2,3,9,14] regarding the role of fingering instabilities on the magnitude of the adhesion force, an analytical model that properly describes such an effect is still lacking. The existing analytical prediction based on a stable retracting circle assumption, and on the sole action of viscous forces, is not in satisfactory agreement with experimental measurements [14]. In order to address this relevant matter, in this work we present an analytical model that explicitly incorporates the effects of fingering into the adhesion force expression. As a matter of fact, in addition to fingering effects, we show that a more accurate theoretical description should also include the contributions coming from wetting effects [35–37] and viscous normal stresses [38–40]. The action of the plate-plate geometry confinement is also taken into account. As we will see, the comparison of our analytical results with careful laboratory measurements for the lifting force performed in Ref. [14] shows an improved agreement between theoretical predictions and experimental data.

II. DERIVATION OF THE LIFTING ADHESION FORCE

The physical system is illustrated in Fig. 1. We consider an incompressible fluid of high viscosity η confined between two narrowly spaced, parallel plates. The outer fluid has negligible viscosity. The upper plate of the probe-tack apparatus is

*jme@df.ufpe.br

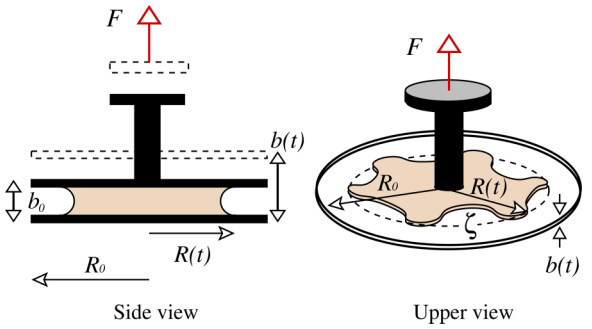

FIG. 1. (Color online) Representative sketch of the lifting flow arrangement in a (plate-plate) probe-tack apparatus.

subjected to a pulling force F so that the plate-plate separation evolves linearly in time according to $b = b(t) = b_0 + Vt$, where V is a constant lifting velocity, and b_0 is the initial plate-plate distance. The z axis is defined in a direction perpendicular to the plates, and the lower plate is held fixed at $z = 0$. The radius of the fluid-fluid unperturbed interface at $t = 0$ is denoted by R_0. The main goal in this section is to calculate the pulling force F as a function of displacement b, taking into account the viscous fingering instability, the effect of a thin wetting film trailing behind the stretched fluid, and viscous normal stress contributions.

We generalize the approach employed by Derks *et al.* [2], where it is assumed that the fluid-fluid interface remains circular during the entire lifting process. Our study is motivated by the fact that the experiments showing fingering instabilities in Refs. [2,3,9,14] are not very well described by theoretical force-distance curves, which consider a stable retracting circle. By considering the action of fingering, the perturbed two-fluid interface is defined as

$$\mathcal{R}(\theta,t) = R(t) + \zeta(\theta,t), \tag{1}$$

where

$$\zeta(\theta,t) = \sum_{n-\infty}^{+\infty} \zeta_n(t) \exp(in\theta) \tag{2}$$

represents the net interfacial perturbation in polar coordinates (r,θ) with Fourier amplitudes $\zeta_n(t)$, and integer azimuthal wave numbers n. $R = R(t)$ is the time-dependent unperturbed radius, which by volume conservation satisfies the relation $R^2\, b = R_0^2\, b_0$.

For the confined plate-plate geometry, inertial effects can be neglected and the governing hydrodynamic equations are Darcy's law [14,19,20,27],

$$\mathbf{v} = -\frac{b^2}{12\eta}\nabla p, \tag{3}$$

and a modified incompressibility condition [19],

$$\nabla \cdot \mathbf{v} = -\frac{\dot{b}}{b}, \tag{4}$$

where the overdot denotes a total time derivative. Remember that in this work, as in most experiments, we take $\dot{b} = V$. In these equations $\mathbf{v} = \mathbf{v}(r,\theta)$ and $p = p(r,\theta)$ are, respectively, the gap-averaged velocity and pressure in the fluid.

From Eqs. (3) and (4) it can be readily verified that the pressure field obeys the Poisson equation

$$\nabla^2 p = \frac{12\eta\dot{b}}{b^3}, \tag{5}$$

whose solution is

$$p(r,\theta) = \frac{3\eta\dot{b}}{b^3}r^2 + \sum_{n\neq 0} p_n(t)\left(\frac{r}{R}\right)^{|n|} e^{in\theta}. \tag{6}$$

Note that previous analytical calculations for the adhesion force do not consider the role of fingering, so that the second term of Eq. (6) is neglected.

To take into account the role of the Saffman-Taylor instability, we have to find a relation between $p_n(t)$ and the perturbation amplitude $\zeta_n(t)$. To obtain such a relation we apply the kinematic boundary condition, which connects the velocity of the lifted fluid with the motion of the interface itself [33]:

$$\frac{\partial \mathcal{R}}{\partial t} = \left[v_r - \frac{1}{r}\frac{\partial \mathcal{R}}{\partial \theta}v_\theta\right]_{r=\mathcal{R}}. \tag{7}$$

Here v_θ and v_r are the azimuthal and radial components of the fluid velocity, respectively. From this point on we employ a perturbative approach by keeping terms up to second order in ζ [32,41]. By expanding Eq. (7), and then Fourier transform, we get

$$\begin{aligned} p_n(t) = \frac{12\eta}{b^2}\Bigg\{ &-\frac{R}{|n|}\dot{\zeta}_n(t) - \frac{\dot{b}R}{2b|n|}\zeta_n(t) \\ &+ \sum_{n'\neq 0}\left[sgn(nn') - \frac{1}{|n|}\right]\dot{\zeta}_{n'}\zeta_{n-n'} \\ &+ \frac{\dot{b}}{2b}\sum_{n'\neq 0}\left[sgn(nn') - \frac{1}{|n|}\right]\zeta_{n'}\zeta_{n-n'}\Bigg\}. \end{aligned} \tag{8}$$

To include the contributions coming from surface tension, viscous normal stresses, and wetting effects, we consider a generalized Young-Laplace pressure boundary condition, which expresses the pressure across the two-fluid interface [15,16,35–38],

$$p|_{r=\mathcal{R}} = \left\{\left[\frac{\pi}{4}\kappa - \frac{2}{b}\right]\sigma - \frac{2J\sigma}{b}\mathrm{Ca}^\gamma + 2\eta\frac{\partial v_r}{\partial r}\right\}\Bigg|_{r=\mathcal{R}}, \tag{9}$$

where, without loss of generality, we set the pressure of the outer fluid to zero. The usual contribution related to surface tension σ and the mean curvature of the fluid-fluid interface is expressed in the first term on the right-hand side of Eq. (9), where κ denotes the interfacial curvature in the plane of the plates [33]. The factor $\pi/4$ is purely a capillary static effect, coming from the z average of the mean interfacial curvature [35,36]. Still in the first term, we have the contribution of the constant curvature $2/b$ associated with the interface profile in the direction perpendicular to the parallel plates.

In this work, we assume that the lifted viscous fluid wets the plates. The second term on the right-hand side of Eq. (9) considers the wetting phenomena [35–37], where $\mathrm{Ca} = \eta v_n/\sigma$ is the capillary number, $J = 3.8$, and $\gamma = 2/3$. Here v_n represents the normal component of the interface fluid velocity that can be written as $v_n = \hat{\mathbf{n}}\cdot\mathbf{v}$, where

$\hat{\mathbf{n}} = \nabla[r - \mathcal{R}(\theta,t)]/|\nabla[r - \mathcal{R}(\theta,t)]|$ denotes the unit normal vector at the interface. Finally, the third term on the right-hand side of Eq. (9) takes into account viscous normal stresses [38–40]. Notice that v_r and v_n can be calculated by Eq. (6), and by Darcy's law, Eq. (3).

The force required to lift the probe-tack apparatus is calculated by integrating the pressure difference above and below the upper plate over the region occupied by the fluid. Therefore, the adhesion force is given by [9]

$$F(t) = -\int_{\Omega(t)} p dA = \frac{1}{2}\int_{\Omega(t)} \nabla p \cdot \mathbf{r} dA - \frac{1}{2}\int_{\Gamma(t)} p\hat{\mathbf{n}} \cdot \mathcal{R}\hat{\mathbf{r}} dl, \quad (10)$$

where $\mathbf{r}$ is a position vector in the plane of the plates (x-y plane). Note that in Eq. (10), we represent the force exerted by the lifting machine on the upper plate by two contributions: one comes from the bubble cross-section in x-y plane $\Omega(t)$, and another one from its time-dependent boundary $\Gamma(t)$.

To obtain the final expression of the pulling force we have to substitute the pressure field Eq. (6), and the fluid pressure at the interface Eq. (9) into the first and second integrals in Eq. (10), respectively. So, keeping terms up to second order in ζ, we have

$$F(t) = f(t) + f_s(t) + Jf_w(t) + \sum_{n\neq 0}[g(t) + g_s(t) + Jg_w(t)]|\zeta_n(t)|^2, \quad (11)$$

where

$$f(t) = \frac{3\pi\eta\dot{b}}{2b^3}R^4, \quad (12)$$

$$f_s(t) = \frac{\pi\eta\dot{b}}{b}R^2, \quad (13)$$

$$f_w(t) = \frac{2\pi\sigma}{b}R^2\left(\frac{\eta\dot{b}}{2\sigma b}R\right)^{\gamma}, \quad (14)$$

$$g(t) = -\frac{12\pi\eta}{b^2}\lambda(n)R^2, \quad (15)$$

$$g_s(t) = -2\pi\eta|n|(n-1)\left[\lambda(n) + \frac{\dot{b}}{2b}\right], \quad (16)$$

and

$$g_w(t) = \frac{\gamma f_w(t)}{2R^2}\left\{1 - n^2 + \lambda(n)\frac{2b}{\dot{b}}\left[(\gamma-1)\lambda(n)\frac{2b}{\dot{b}} - 2\right]\right\}. \quad (17)$$

In Eqs. (11)–(17) the subscripts s and w identify the terms related to viscous normal stresses and wetting effects, respectively.

In addition, in Eqs. (15)–(17), $\lambda(n)$ denotes the time-dependent, linear growth rate of the amplitudes $\zeta_n(t)$, which is given by [31,32]

$$\lambda(n) = \frac{1}{s(n) + w(n)}\left\{\frac{\dot{b}}{2b}[|n| - s(n)] - \frac{\pi\sigma b^2}{48\eta R^3}|n|(n^2-1)\right\}, \quad (18)$$

where

$$s(n) = 1 + \frac{b^2}{6R^2}|n|(|n|-1) \quad (19)$$

is associated to the effects of the viscous normal stresses, and

$$w(n) = \gamma|n|J\frac{b}{6R}\left(\frac{2b\sigma}{\dot{b}\eta R}\right)^{1-\gamma} \quad (20)$$

is related to the wetting film contribution. It is worthwhile to note that, consistent with experimental findings, we have verified that for the strongly confined very viscous fluids used here and in Refs. [2,3,9,14], the contribution of capillary effects [terms between square brackets in Eq. (9)] to the adhesion force Eq. (11) is very small and can be neglected. However, capillary effects are of relevance for the calculation of the interfacial perturbation amplitudes $\zeta_n(t)$, and for the terms connected to them in Eq. (11) [$g(t)$, $g_s(t)$, and $g_w(t)$].

The adhesion force Eq. (11) is our central analytical result. In the equation, $f(t)$ corresponds to the traditional theoretical model (hereafter referred to as the "simplest model") of the adhesion force, which only includes the contributions of viscous effects [2,3,9,14]. All the remaining terms of Eq. (11) are associated with the additional physical contributions we consider in our current theoretical model. Observe from Eq. (11) that the functions $g(t)$, $g_s(t)$, and $g_w(t)$ couple with the fingering term $|\zeta_n(t)|^2$. Finally, note that to obtain the complete dependence of the force on time, we have to know the evolution of the perturbations amplitudes $\zeta_n(t)$. The dynamics of these disturbances has been recently studied in Refs. [31,32], where Darcy's law, Eq. (3), incompressibility Eq. (4), and boundary condition Eqs. (7) and (9) are used to obtain a differential equation for the evolution of the perturbation amplitudes $\dot{\zeta}_n(t) = \lambda(n)\zeta_n(t) + O(\zeta^2)$, yielding

$$\zeta_n(t) = \zeta_n(0)\exp\left[\int_0^t \lambda(n)dt'\right]. \quad (21)$$

III. DISCUSSION AND COMPARISON WITH EXPERIMENTS

In this section we contrast the experimental data obtained in the paper by Nase *et al.* [14] for the lifting adhesion force with the theoretical predictions of the analytical model we have developed in this work [Eq. (11)]. These set of data are also compared to the simplest model of the adhesion force [Eq. (12)] [2,3,9,14], which only includes the contributions of viscous effects, and neglects fingering, viscous normal stresses, and wetting effects. To facilitate the comparison of our model with the experimental findings presented in Ref. [14], we define the dimensionless quantities

$$t' = \frac{V}{b_0}t, \quad \tau_0 = \frac{\sigma b_0^3}{12\eta V R_0^3}, \quad \text{and} \quad q = \frac{R_0}{b_0}, \quad (22)$$

where t' is a reduced time, τ_0 is a surface tension parameter, and q is the initial aspect ratio (measure of the system's

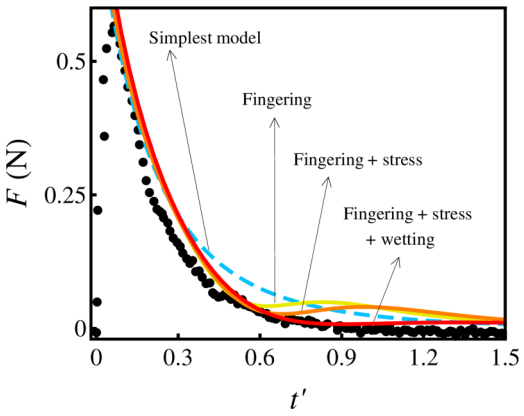

FIG. 2. (Color online) Lifting adhesion force F plotted as a function of the reduced time t' for aspect ratio $q = 54.5$, and surface tension parameter $\tau_0 = 3.0 \times 10^{-5}$. Here at $t = 0$, $n_c = 145$. The dashed curve represents the results obtained by the simplest model [2,3,9,14]. The experimental points (•) are from Nase *et al.* [14]. The three solid curves all refer to the situation described by the analytical model we develop in this work, gradually including the various physical effects we took under consideration: first, only fingering, then fingering plus viscous normal stress, and finally fingering plus stress, plus wetting.

confinement). These are the parameters utilized in the experimental investigation carried out in Ref. [14].

We begin our discussion by examining the representative Fig. 2, which depicts how the adhesion force F (measured in Newtons) varies as a function of the dimensionless reduced time t'. We stress that this is exactly the way the experimental data has been presented in Nase *et al.* [14] (see their Fig. 14). Throughout this section, the characteristic physical parameters we used are precisely those utilized in Ref. [14], namely: $\eta = 100$ Pa s, $\sigma = 0.02$ N/m, and $R_0 = 3.0$ mm. The same is true for values we consider for the aspect ratio q. In Fig. 2 we take $q = 54.5$ and surface tension parameter $\tau_0 = 3.0 \times 10^{-5}$. All initial perturbation amplitudes $\zeta_n(0)$ we used are of the order of 10^{-7}–10^{-6} m. In our calculations, the participating wave numbers are $0 \leqslant n \leqslant n_c$, where n_c is the critical mode at $t = 0$. This critical mode is obtained by setting $\lambda(n = n_c) = 0$ [see Eq. (18)], establishing the width of the band of unstable modes.

Figure 2 presents the experimental data points taken from Ref. [14] (represented by the symbol •) and four theoretical curves. A typical experimental curve as the one represented by the data points in Fig. 2 starts with a sharp increase of the adhesion force once the probe is pulled apart. The force quickly reaches its maximum and then drops asymptotically to zero as the plate-plate separation is increased. It has been shown [1–4,8] that the formation of a sharp peak is due to the compliance of the lifting apparatus. Here, as in Refs. [2,3,9,14], without loss of generality, we consider an infinitely rigid machine, where the force starts at a finite value and eventually tends to zero as the plate separation increases (as represented by the four theoretical curves in Fig. 2).

Regarding the theoretical curves illustrated in Fig. 2, the dashed curve is related to the results obtained by the simplest model [2,3,9,14], while the three solid curves are related to the results acquired from our analytical model for the adhesion force, progressively including the relevant physical ingredients (fingering, normal stresses, and wetting). The first solid curve just adds the contribution of fingering, the second considers the action of fingering and viscous normal stress, and finally the third one takes into account the joined effects of fingering, viscous normal stress, and wetting. This is done to illustrate the contribution of each physical ingredient in shaping the ultimate form of the adhesion force curve.

By examining Fig. 2 we notice that there is a clear discrepancy between the dashed curve (representing the simplest model) and the experimental data. In order to get a better fit, we start adding the new ingredients considered by our model. First, we add just the effect coming from fingering to the simplest model: as one can verify from Fig. 2 the addition of fingering approaches the theoretical curve to the experimental data for intermediate values of t' ($0.4 < t' < 0.6$). However, the solid curve associated to the fingering contribution presents a bump for larger values of t' ($t' > 0.6$). This bump is not in agreement with the experimental points. This indicates that by perturbatively adding just the action of fingering, one does not get a good fitting with the experimental data, at least for larger reduced times. The unphysical overshoot observed in Fig. 2 when only fingering is considered reinforces the importance of the coupling between fingering, normal stresses, and wetting expressed in Eq. (11). If just fingering is taken into account, the adhesion force is overestimated for larger times. In a recent work [31], two of us have shown that the predictions for the number of fingers in the lifting Hele-Shaw cell improve significantly when one takes into account the role played by viscous normal stresses and by wetting film effects. These stresses are related to normal velocity gradients at the fluid-fluid interface [38–40]. On the other hand, it is known the thin layer of oil (inner fluid) left on the plates [35–37] could explain the fact that the adhesion force is smaller than predicted from the simplest model theory [14]. It is precisely the stabilizing role of both normal stresses and wetting that prevents the mentioned unphysical overshoot behavior when all these effects (fingering, normal stresses, and wetting) act simultaneously.

Motivated by these findings [14,31,35–40], first we decided to consider the combined effect of fingering and stress (see Fig. 2). One effect we see is that the normal viscous stresses tend to lower the intensity of the nonphysical bump that arises at larger t' values. However, a smaller bump still persists. At this point, a logical alternative would be to consider the effect of the wetting film left behind during the lifting process. This is represented by the solid curve in Fig. 2 that implements our model, now taking into account the role of fingering, viscous normal effects, and wetting. By inspecting Fig. 2 it is evident that the inclusion of all these ingredients make the unphysical bump disappear, leading to a much better fit between experimental data and our theoretical model. We emphasize that the general findings and conclusions presented above for the illustrative case depicted in Fig. 2 have also been observed in all other cases considered in this work, which assumed different values of τ_0 and q. In order to substantiate the effectiveness and greater accuracy of our analytical model for the lifting adhesion force (as illustrated by Fig. 2), below we present a series of results for other values of the aspect ratio q, and two characteristic values of the surface tension parameter τ_0.

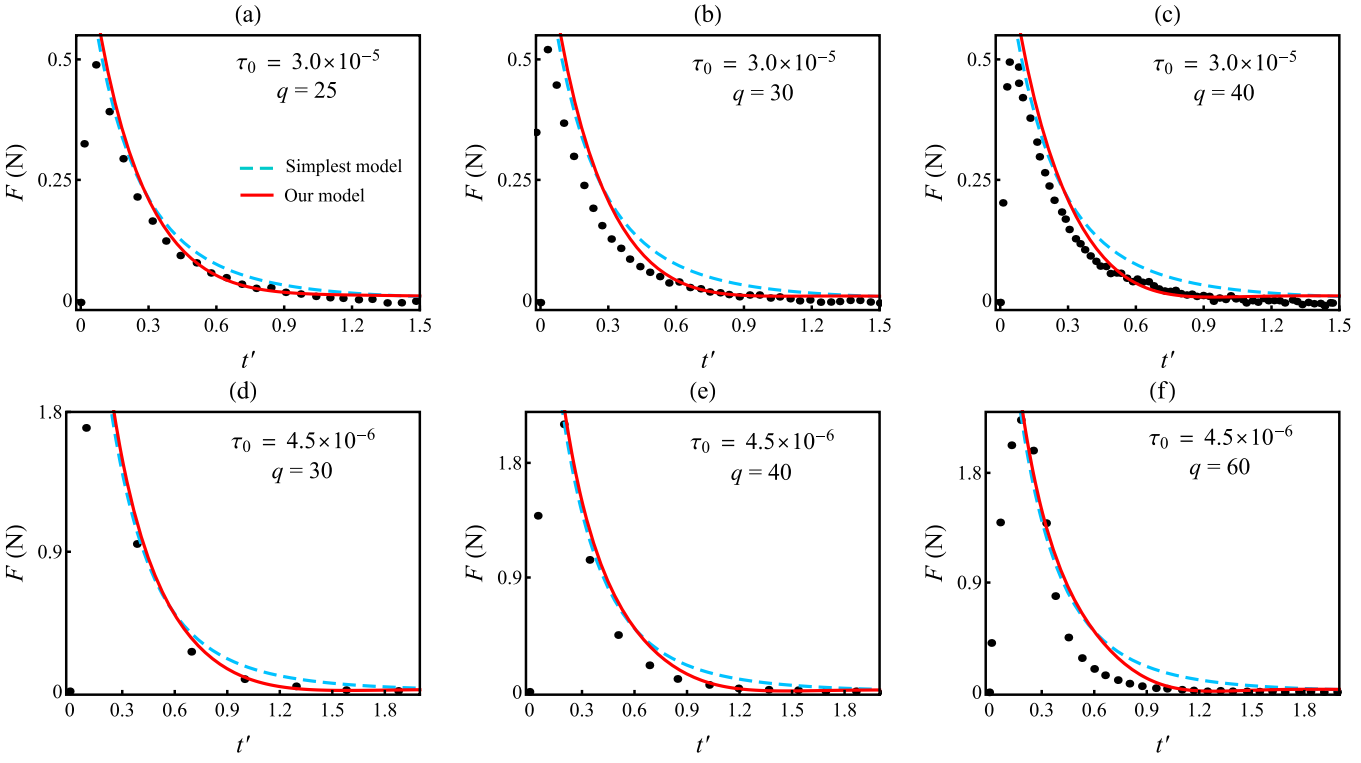

FIG. 3. (Color online) Adhesion force F as a function of the reduced time t', for several values of the aspect ratio q, and two values of the surface tension parameter τ_0 : 3.0×10^{-5} [(a)–(c)], and 4.5×10^{-6} [(d)–(f)]. In panels (a)–(c), $n_c = 145$ at $t = 0$, while in panels (d)–(f), $n_c = 360$ at $t = 0$. The theoretical curves refer to the adhesion force calculated from the simplest model used in Refs. [2,3,9,14] (dashed curves), and from our current model that takes into consideration the combined influence of fingering, wetting, and viscous normal stresses (solid curves). The experimental points (•) are from Fig. 14 in Nase *et al.* [14].

We proceed our discussion by analyzing Fig. 3, which plots the adhesion force F in terms of the reduced time t'. The dashed curves refer to the simplest model utilized in Refs. [2,3,9,14], while the solid curves are obtained from our model. Once again, the experimental data have been taken from Nase *et al.* [14] (more precisely from their Fig. 14) and are represented by the solid black circles (•). Figures 3(a)–3(c) consider an effective surface tension parameter $\tau_0 = 3.0 \times 10^{-5}$ and increasingly larger values for the aspect ratios (a) $q = 25$, (b) $q = 30$, and (c) $q = 40$. These are precisely the values of τ_0 and q used in Fig. 14(a) of Ref. [14]. On the other hand, Figs. 3(d)–3(f) take a smaller value for τ_0 ($\tau_0 = 4.5 \times 10^{-6}$) and aspect ratios (d) $q = 30$, (e) $q = 40$, and (f) $q = 60$. Now, the values of τ_0 and q utilized in Figs. 3(d)–3(f) are exactly the ones used in Fig. 14(b) of Ref. [14].

First, we inspect Figs. 3(a)–3(c). As verified by the experiments performed in Ref. [14], larger values of τ_0 are associated to a less destabilized interface, resulting in patterns presenting a smaller number of fingers. So, in principle, the effects of fingering should not be dramatic in Figs. 3(a)–3(c). Moreover, as also experimentally observed in Ref. [14], larger values of q (larger confinement) lead to greater interface destabilization and consequently to the production of more fingers. Therefore, for a fixed τ_0 the role of fingering on adhesion should become more relevant as q assumes larger values.

By examining Figs. 3(a)–3(c) we see that the experimental results lie below the dashed curve that is calculated from the simplest model. On the other hand, it is also evident that the solid curve obtained from our model presents regions where one finds an improved fit with the experimental data, notably where t' is not very small. This is indicative of the fact that our analytical modeling for the adhesion force, where the contributions of fingering, wetting, and viscous normal stresses are of relevance, provides a better agreement with existing experimental measurements.

At early reduced times, note that both curves (dashed and solid) overlap and are situated considerably above the first few experimental points. Nevertheless, this is not really surprising. As we mentioned earlier, it is known that at the initial time regime the peak behavior shown by the experimental data is attributed to the compliance (or, stretching) of the probe-tack apparatus [1–3,9,14]. The effect of the apparatus' compliance is not considered in either theoretical models (simplest or ours), so this can at least partially justify the mismatch between both theories and the experimental data for small t'. It is worth noting that as q is increased the dashed curve tends to get away from the data points, while the solid curve stick close to them, supporting the relevance of the various effects included in our model to better describe the experiments.

At this point, we turn to the analysis of Figs. 3(d)–3(f). Recall that now we are considering growing aspect ratios q under a lower value of τ_0 as compared to the one utilized in Figs. 3(a)–3(c). Thus, a greater number of longer fingers should arise at the fluid-fluid interface [14]. In these circumstances, one should expect that the effect of fingering on the adhesion force should be even more important. In fact, this is what one verifies

by examining Figs. 3(d)–3(f): the distance found between the experimental data points and the computed forces (for both models, simplest and ours) tend to increase as q is increased. Nonetheless, as in Figs. 3(a)–3(c) we see that the the solid curves still provide a better match with the data. This is particularly true when the aspect ratio $q = 30$ and 40. However, the agreement is not so good for $q = 60$. This can be explained by the fact that our analytical model is based on a perturbative approach, which is valid only for small interfacial perturbation amplitudes. Higher values of q quickly produce fingers with sizable amplitudes, a situation that is beyond the validity of our analytical model. Despite this limitation, our theoretical results still offer a better agreement with the experiments.

We close this section by providing a more quantitative basis to the improved agreement of our model with the experimental data, as contrasted with the simplest model employed in Refs. [2,3,9,14]. In order to do that we utilized the Kolmogorov-Smirnov test [42,43] using the data plotted in Fig. 3. Since both our model and the simplest model do not consider the compliance of the probe-tack apparatus, we have excluded all data points appearing prior to the force peak. This statistical test is very common in the fields of science and engineering, and is quite useful when one wishes to compare two sets of measurements. For a comprehensive treatment about this test, see, e.g., Ref. [44]; for computational details, see Refs. [44,45].

Consider two theoretical models for which the hypothesis "the theoretical model fits the experimental data" cannot be rejected. For the two cases, the so-called p value obtained by a goodness-of-fit test (as the Kolmogorof-Smirnov test) is greater than a previous to test chosen significance level α (a usual choice is $\alpha = 0.05$, to have a test with a confidence level equal to 95%). In this context, we should select as the best model, that model associated with the larger p value. The results obtained for the calculated p values (by applying the Kolmogorov-Smirnov test) to verify the goodness of fit with the experimental data from Ref. [14] [as plotted in Figs. 3(a)–3(f)] are presented in Table I. First, we show the p values applying the test for the experimental data [14], and the corresponding data obtained from our model (Exp., ours). In the following row of the table, we display the p values associated with the test used by considering the experimental data, and the corresponding data extracted from the simplest model [2,3,9,14] (Exp., simplest). Within the scope of the Kolmogorov-Smirnov test the results displayed in Table I indicate that our analytical model does provide a better fit with experimental data.

TABLE I. p values associated with the data contained in Figs. 3(a)–3(f). Significance level of the Kolmogorov-Smirnov test: $\alpha = 0.05$. The best model is the one associated with the largest p value.

	p values					
Fig. 3	(a)	(b)	(c)	(d)	(e)	(f)
Exp., ours	0.5713	0.9180	0.9821	0.9999	0.9971	0.9205
Exp., simplest	0.5713	0.0887	0.1340	0.9627	0.4792	0.1549

IV. CONCLUDING REMARKS

Sophisticated numerical simulations and careful experimental measurements indicate that the lifting adhesion force obtained for probe-tack tests with fluids is influenced by the fingering instabilities that develop at the contracting two-fluid interface. Traditional analytical modeling of the situation (the simplest model) does not take into consideration the effect of the fingering patterns on the adhesion force strength. Consequently, there exists a mismatch between existing analytical predictions for adhesion force and actual experimental data.

In this work, we proposed an enhanced analytical description for the adhesion force that adds to the simplest model not only the effects of fingering but also the influence of viscous normal stresses and the action of the wetting film left behind on the plates of the lifting apparatus. By comparing our analytical results with existing experimental data, we showed that the successive addition of these three contributions (fingering, normal stresses, and wetting) leads to increasingly improved theoretical predictions for the adhesion force. Such comparisons have been performed for two values of the surface tension parameter, and several values of the plate-plate confinement (aspect ratio q of the system). Employment of the Kolmogorov-Smirnov statistical test supports the idea that our analytical model does work better than the simplest model in describing the actual behavior of the system as expressed by experiments.

ACKNOWLEDGMENTS

We thank CNPq and FACEPE (through PRONEM Project No. APQ-1415-1.05/10) for financial support. We are grateful to Julia Nase for kindly supplying the experimental adhesion force data of Ref. [14].

[1] B. A. Francis and R. G. Horn, J. Appl. Phys. **89**, 4167 (2001).
[2] D. Derks, A. Lindner, C. Creton, and D. Bonn, J. Appl. Phys. **93**, 1557 (2003).
[3] S. Poivet, F. Nallet, C. Gay, and P. Fabre, Europhys. Lett. **62**, 244 (2003).
[4] M. Tirumkudulu, W. B. Russel, and T. J. Huang, Phys. Fluids **15**, 1588 (2003).
[5] R. D. Welsh, M.Sc. thesis, Massachusetts Institute of Technology, 2001.
[6] J. A. Miranda, Phys. Rev. E **69**, 016311 (2004).
[7] J. A. Miranda, R. M. Oliveira, and D. P. Jackson, Phys. Rev. E **70**, 036311 (2004).
[8] S. Poivet, F. Nallet, C. Gay, J. Teisseire, and P. Fabre, Eur. Phys. J. E **15**, 97 (2004).
[9] A. Lindner, D. Derks, and M. J. Shelley, Phys. Fluids **17**, 072107 (2005).
[10] Y. O. M. Abdelhaye, M. Chaouche, and H. Van Damme, Appl. Clay Sci. **42**, 163 (2008).
[11] S. A. Lira and J. A. Miranda, Phys. Rev. E **80**, 046313 (2009).

[12] Q. Barral, G. Ovarlez, X. Chateau, J. Boujlel, B. Rabideau, and P. Coussot, Soft Matter **6**, 1343 (2010).
[13] R. H. Ewoldt, P. Tourkine, G. H. McKinley, and A. E. Hosoi, Phys. Fluids **23**, 073104 (2011).
[14] J. Nase, D. Derks, and A. Lindner, Phys. Fluids **23**, 123101 (2011).
[15] E. O. Dias and J. A. Miranda, Phys. Rev. E **85**, 016312 (2012).
[16] E. O. Dias and J. A. Miranda, Phys. Rev. E **86**, 046322 (2012).
[17] A. Zosel, Colloid Polym. Sci. **263**, 541 (1985).
[18] H. Lakrout, P. Sergot, and C. Creton, J. Adhes. **69**, 307 (1999).
[19] M. J. Shelley, F.-R. Tian, and K. Wlodarski, Nonlinearity **10**, 1471 (1997).
[20] J. Bohr, S. Brunak, and T. Nørretranders, Europhys. Lett. **25**, 245 (1994).
[21] S. Roy and S. Tarafdar, Phys. Rev. E **54**, 6495 (1996).
[22] S. K. Thamida, P. V. Takhistov, and H.-C. Chang, Phys. Fluids **13**, 2190 (2001).
[23] S. Sinha, S. K. Kabiraj, T. Dutta, and S. Tarafdar, Eur. Phys. J. B **36**, 297 (2003).
[24] S. K. Kabiraj and S. Tarafdar, Physica A **328**, 305 (2003).
[25] J. A. Miranda and R. M. Oliveira, Phys. Rev. E **69**, 066312 (2004).
[26] C.-Y. Chen, C.-H. Chen, and J. A. Miranda, Phys. Rev. E **71**, 056304 (2005).
[27] M. Ben Amar and D. Bonn, Physica D **209**, 1 (2005).
[28] J. Nase, A. Lindner, and C. Creton, Phys. Rev. Lett. **101**, 074503 (2008).
[29] S. Sinha, T. Dutta, and S. Tarafdar, Eur. Phys. J. E **25**, 267 (2008).
[30] E. O. Dias and J. A. Miranda, Phys. Rev. E **81**, 016312 (2010).
[31] E. O. Dias and J. A. Miranda, Phys. Rev. E **88**, 043002 (2013).
[32] P. H. A. Anjos and J. A. Miranda, Soft Matter **10**, 7459 (2014).
[33] G. M. Homsy, Annu. Rev. Fluid Mech. **19**, 271 (1987); K. V. McCloud and J. V. Maher, Phys. Rep. **260**, 139 (1995).
[34] P. G. Saffman and G. I. Taylor, Proc. R. Soc. London Ser. A **245**, 312 (1958).
[35] C.-W. Park and G. M. Homsy, J. Fluid Mech. **139**, 291 (1984).
[36] L. Schwartz, Phys. Fluids **29**, 3086 (1986).
[37] P. H. A. Anjos and J. A. Miranda, Phys. Rev. E **88**, 053003 (2013).
[38] E. Alvarez-Lacalle, J. Ortín, and J. Casademunt, Phys. Fluids **16**, 908 (2004).
[39] H. Gadêlha and J. A. Miranda, Phys. Rev. E **79**, 066312 (2009).
[40] H. Kim, T. Funada, D. D. Joseph, and G. M. Homsy, Phys. Fluids **21**, 074106 (2009).
[41] J. A. Miranda and M. Widom, Physica D **120**, 315 (1998).
[42] A. N. Kolmogorov, G. Ist. Ital. Att. **4**, 83 (1933).
[43] N. Smirnov, Ann. Math. Stat. **19**, 279 (1948).
[44] M. G. Kendall and A. Stewart, *The Advanced Theory of Statistics*, 3rd ed. (Hafner, New York, 1973), Vol. 2.
[45] W. H. Press, B. P. Flannery, S. A. Teukolsky, and W. T. Vetterling, *Numerical Recipes: The Art of Scientific Computing* (Cambridge University Press, Cambridge, England, 1986).